American Mineralogist, Volume 78, pages 775–781, 1993

Structure of magnesian calcite from sea urchins

SEMEON J. TSIPURSKY, PETER R. BUSECK
Departments of Geology and Chemistry, Arizona State University, Tempe, Arizona 85287-1404, U.S.A.

ABSTRACT

X-ray θ scans and high-resolution transmission electron microscopy (HRTEM) imaging indicate that the calcite of sea urchin spines and skeletal plates forms in mosaic crystals. Both coherent and incoherent boundaries were observed between slightly misaligned crystallites. Small domains show an ordered superstructure. Using HRTEM and both X-ray and electron diffraction data, we found that the most appropriate model for this superstructure has Ca:Mg = 3:1 and alternating Ca layers and Ca and Mg layers along **c**. We did not find evidence for the presence of protein molecules within the calcite structure.

INTRODUCTION

Numerous organisms produce calcium carbonate crystals in the oceanic environment, and the resulting biogenic minerals are important contributors to carbonate sediments on the ocean bottom (Lowenstam and Weiner, 1989). Being abundant in sediments, these carbonates are involved in diagenetic processes, and their complete characterization is important for understanding the changes that occur during diagenesis. Echinoderms, consisting of magnesian calcite, are prominent sources of carbonates and are the focus of this study.

In spite of extensive investigations of echinoid hard parts, details of their structure are still not known with certainty. Some scientists consider them to consist of single crystals (Raup, 1966; Donnay and Pawson, 1969; Nissen, 1969), whereas others believe they are polycrystals (Pearse and Pearse, 1975; O'Neil, 1981). Towe (1967) proposed that echinoderm skeleton elements are a combination of both single crystals and polycrystalline aggregates. Using high-resolution transmission electron microscopy (HRTEM), Blake et al. (1984) concluded that echinoderm calcite consists of a pervasive mosaic structure that crystallized "under strong organism control." Paquette and Reeder (1990) obtained single-crystal X-ray structure refinements of echinoderm magnesian calcite, and, in contrast to dolomite, they found no evidence for Mg ordering.

An intriguing feature, and one that has given rise to considerable speculation, is the unusual flexibility and strength of echinoderm calcite. Its mechanical properties have been explained by either the porous character or the hypothesized composite nature of the calcite. Currey (1975), Burkhardt and Märker (1979), and Emlet (1982) proposed that it is the porous structure that improves properties such as flexural, torsional, buckling, and tensile strengths. On the other hand, Berman et al. (1990) suggested, by analogy with composite materials, that protein molecules intergrown within the calcite are the critical factors, although Currey and Nichols (1967) and Kleyn and Currey (1970) reported an absence of organic material in echinoderm calcite.

There are unresolved differences of opinion regarding biogenic calcite. The purpose of the present investigation is to examine echinoderm hard parts to obtain information about their structural states and to search for evidence of protein molecules within the biogenic crystals that would indicate their composite character. We used X-ray diffraction, electron microprobe analysis, and transmission electron microscopy to study spines and skeleton plates of *Strongylocentrotus franciscanus* (*Str. fr.*), a deep water species, and *Strongylocentrotus purpuratus* (*Str. pr.*), a shallow water species.

EXPERIMENTAL

Plates and spines of *Str. fr.* and *Str. pr.* were obtained from fresh specimens. They were studied using a D/MAX-IIB Rigaku X-ray diffractometer, operated at 50 keV, 30 mA, and equipped with a Cu$K\alpha$ source, curved graphite monochromator, and a 0.15° receiving slit. Samples for electron microscopy were oriented using X-ray diffraction measurements, and then thin sections parallel and perpendicular to the [001] direction were cut, ground to a 30-μm thickness, and ion milled. Microscopy was performed using a Jeol JEM-4000EX electron microscope at a 400-keV accelerating voltage and with a point to point resolution of 0.17 nm. A 45-μm objective aperture and 150-μm condenser aperture were used.

Chemical analyses were obtained with an automated electron microprobe analyzer (Jeol-JXA 8600 Superprobe) using wavelength-dispersive spectroscopy. Samples were mounted on glass slides, polished, and coated by vacuum evaporation with a thin conducting layer of C. The microprobe was operated at 15 kV and 10 nA, with a 15-μm spot size. Count integration was for 30 s for Mg and 5 s for Ca.

X-RAY RESULTS

The positions and intensities of the reflections from powder X-ray diffraction (XRD) patterns of all the mea-

0003–004X/93/0708–0775$02.00

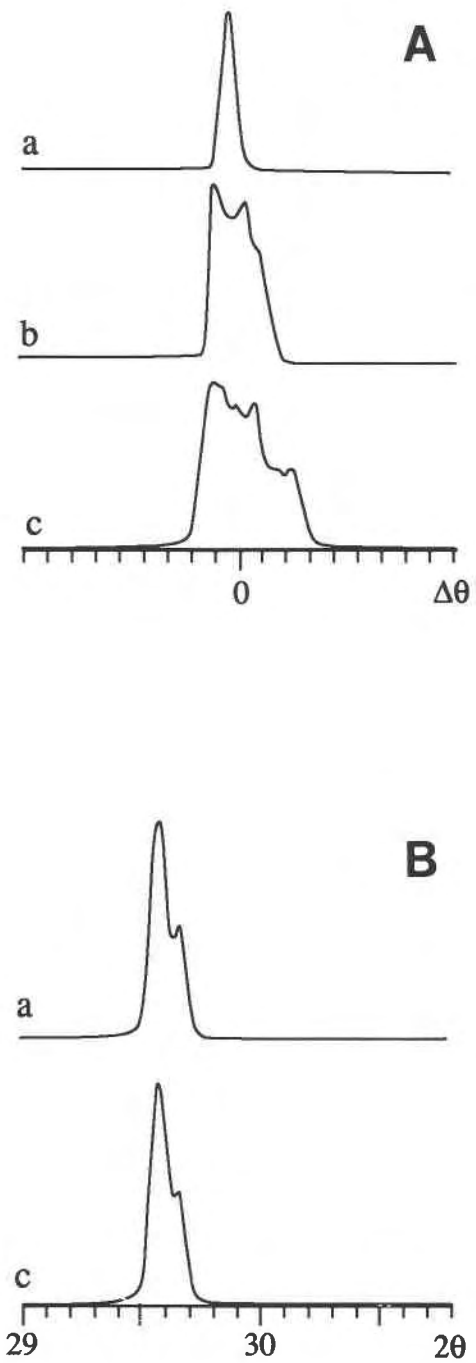

Fig. 1. (A) X-ray θ scans of the 104 reflection from a: a nominally crack-free single crystal of calcite; b: a calcite crystal with one crack visible with an optical microscope, and c: a mosaic calcite crystal. Note the changes in peak shapes within this series. (**B**) The $\theta/2\theta$ scans of the 104 reflection from crystals a and c, above. The increased sensitivity of the θ scans relative to $\theta/2\theta$ scans is evident.

sured samples are typical of calcite. We were interested in assessing the crystal perfection of this calcite. Yukino and Uno (1986) showed that such measurements could be made of either powders or larger crystals through the use of XRD rocking-curve procedures (Azároff et al., 1974), which we will call θ scans to distinguish them from standard $\theta/2\theta$ diffraction scans. During such a θ scan, the specimen is rotated slightly around the axis of an X-ray powder diffractometer, with the X-ray source and detector retained at a fixed 2θ value for a given Bragg peak. This procedure is in contrast to a more conventional $\theta/2\theta$ scan, in which both crystal and detector are rotated synchronously. The resulting diffraction pattern contains information about both the sizes and orientations of the crystals in the specimen (Yukino and Uno, 1986).

Slabs of calcite crystals, roughly 1 × 5 × 5 mm in size, were used as standards to test the θ scan method. Three types of samples were studied: (1) a transparent crystal (Iceland spar) free of cracks visible with an optical microscope, (2) a transparent crystal with a single microscopic crack evident, and (3) a crystal containing multiple microfractures. Slabs 2 and 3 were taken as models of crystals having mosaic structures. The crystals were polished, mounted on glass slides, and then oriented on the X-ray diffractometer.

We obtained both θ and $\theta/2\theta$ scans in order to test which is more sensitive to crystal mosaicism. When using a powder diffractometer to study a nominally single crystal, as we did for these measurements, it is necessary to determine the exact θ orientation of the crystal before obtaining a $\theta/2\theta$ scan. The θ scan profiles of the 104 reflection, produced when a crystal fragment lies on its cleavage surface, were obtained for our three reference crystals (Fig. 1A). The differences in width and peak complexity increase markedly with the extent of imperfections. Having determined the θ position for the 104 peak from the θ scan, conventional $\theta/2\theta$ scans were used to obtain Bragg diffraction spectra (Fig. 1B). In spite of the striking difference among the θ scan patterns (Fig. 1A), a comparison with the $\theta/2\theta$ patterns (Fig. 1B) shows no marked broadening of reflections from a mosaic crystal relative to those from a single crystal. It is evident that θ scans are more sensitive to mosaic structures than are $\theta/2\theta$ scans. Thus, we used θ scans for studying the echinoderm samples.

Structure of sea urchin spines and skeletal parts

Spines of *Str. fr.* and *Str. pr.* were sectioned so that they were both parallel and perpendicular to their lengths for X-ray study. Optical microscopy in both reflected and transmitted light showed that the sections were flat and free of observable fractures. Samples were mounted onto glass slides and oriented in the diffractometer. The 00*l* reflections were obtained for the transverse sections. The θ scans of the 0,0,12 reflection from many samples of *Str. fr.* spines all produced broad, complex, and asymmetric peaks having full widths at half maximum (FWHM) of ~0.9° (Fig. 2A). Having determined the proper θ position for the 0,0,12 reflection, we obtained $\theta/2\theta$ scans. Figure 2B shows the $\theta/2\theta$ scan of the 00*l* reflections of the crystal used for Figure 2A. Similar $\theta/2\theta$ profiles were obtained

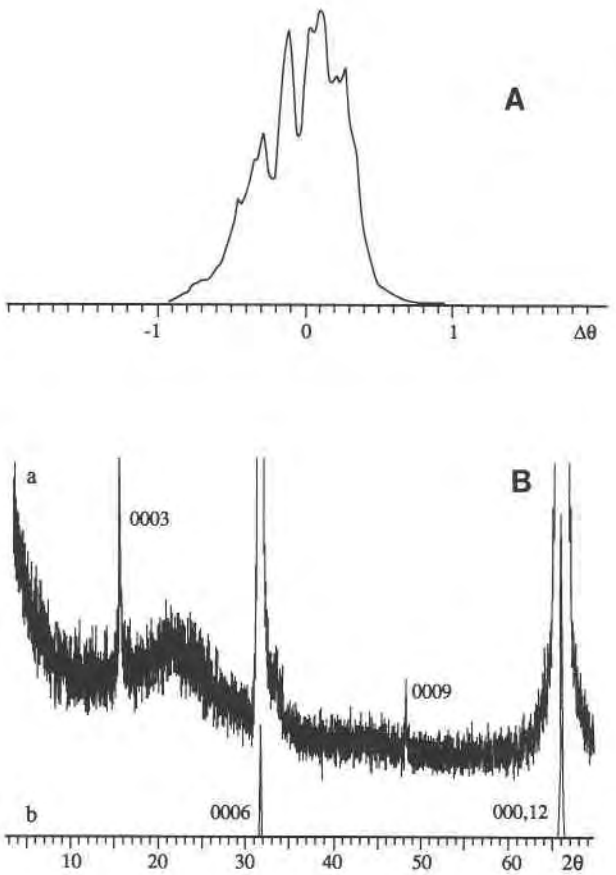

Fig. 2. **(A)** A θ scan of the 0,0,12 reflection of a *Str. fr.* spine. **(B)** A $\theta/2\theta$ scan of the 00*l* reflections of a *Str. fr.* spine, with the two strongest peaks (006 and 0,0,12) shown with intensities scaled so that the peak positions are evident. The intensity of the 003 peak is 300 counts (curve a), whereas that of the strong 0,0,12 peak (b) is 200 000 counts.

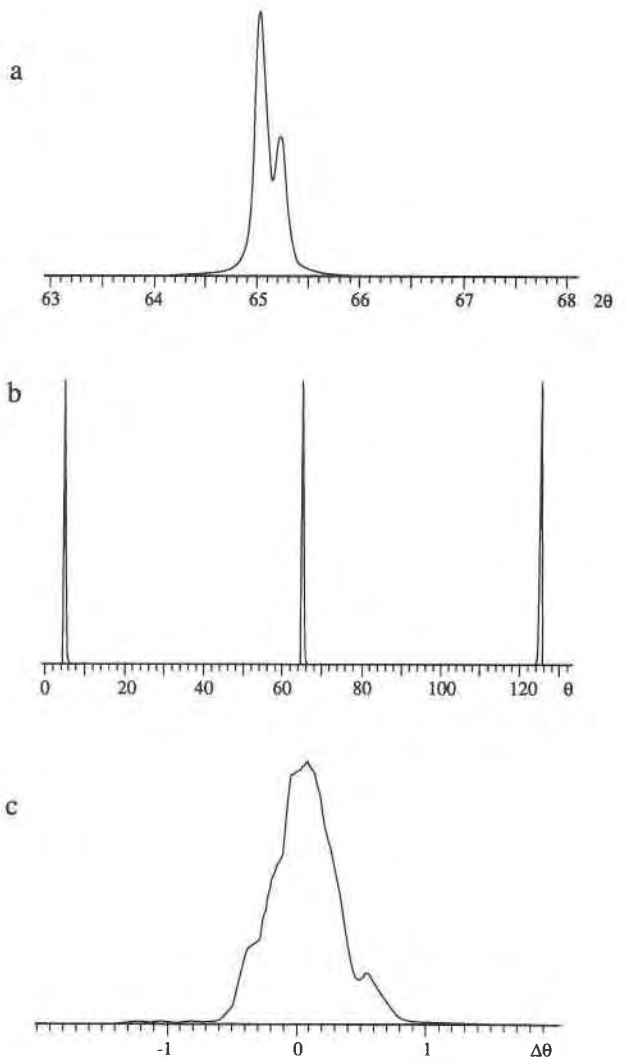

Fig. 3. X-ray scans of 300-type reflections from a *Str. fr.* spine. **(a)** A $\theta/2\theta$ scan of the 300 reflection, **(b)** θ scan of the 300, 030, and $\bar{3}30$ reflections, and **(c)** θ scan of the 300 reflection. The peak width in **c** has been expanded relative to **b** in order to show details within the peak.

when the crystal was oriented for any position within the FWHM range shown in Figure 2A.

Typically, calcite 00*l* and *h*00 reflections are weak on powder XRD patterns because of the preferred orientation along {104} cleavage planes and the correspondingly strong 104 reflections. Our patterns, which are not of powdered samples, show strong, narrow 006 and 0,0,12 peaks, together with weaker 003 and 009 peaks (Fig. 2B). The strong peaks have *d* values of 0.2827(2) and 0.14136(4) nm, and the weak ones have values of 0.5543(6) and 0.18467(7) nm. These peaks are not simple submultiples of a single *c* parameter, presenting an interesting problem. In addition, 003 and 009 reflections are forbidden by the $R\bar{3}c$ space group of calcite. We interpret this situation as one resulting from the superpositioning of reflections that arise from two structures having different symmetries—$R\bar{3}c$ and $R\bar{3}$ (or $C2/m$), with the latter being a minor component. The patterns arise from calcite and dolomite-like structures, with the strong calcite peaks normally obscuring the weak 006 and 0,0,12 dolomite-like peaks. Calculated *c* dimensions corresponding to the two sets of peaks are 1.696 and 1.662 nm, respectively.

In order to examine the effects of mosaicism in other directions, we reoriented the crystals to investigate a set of *h*00 reflections. An entire *Str. fr.* spine was mounted on the XRD goniometer, with the long spine axis coincident with the axis of rotation of the goniometer. By using conventional $\theta/2\theta$ scans around **c**, we found sharp 300 reflections that are well resolved into $K\alpha_1$ and $K\alpha_2$ peaks (Fig. 3a). The θ scans around **c** show three well-defined peaks that are separated by 60° and that result from the {300} planes (Fig. 3b), as is typical of well-developed single crystals. However, there is considerable dispersion (~0.6° FWHM) evident in the θ scans (Fig. 3c), showing that this is, in fact, a mosaic crystal.

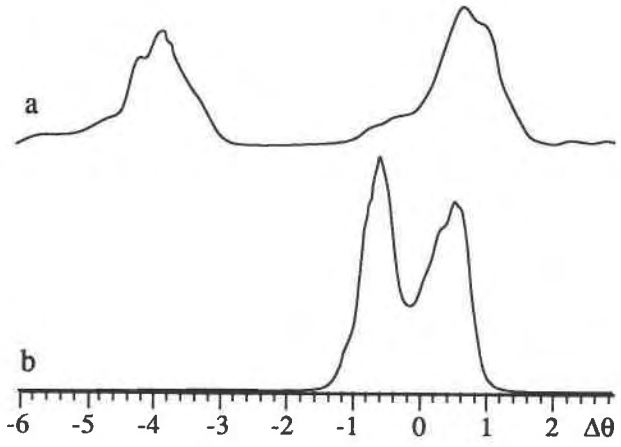

Fig. 4. Two θ scans of the 0,0,12 reflections from *Str. pr.* skeleton plates from a single specimen. Curve a shows two widely separated peaks, and curve b shows two overlapping peaks. Other plates show different peak separations.

The results from skeletal plates differed slightly from those of spines. The θ scans of 0,0,12 reflections show both dispersion (Fig. 4a) and apparent angular separation of up to 5° into distinct crystals, each of which shows distinct mosaicism (Fig. 4b). Close examination of Figure 4 shows additional minor structural complexity in the weak peripheral peaks.

Analytical and TEM observations

All of the calcite that we analyzed is magnesian. Based on a series of electron microprobe measurements, we estimate the $MgCO_3$ content as ranging from 2.4 to 4.5 mol% for spines of *Str. pr.* and *Str. fr.* and for skeletal plates of *Str. fr.* and $MgCO_3$ content from 4.2 to 7.8 mol% for skeletal plates of *Str. pr.* The estimated error for any given analysis is about 3% (relative) for Mg and about 1% for Ca. Neither systematic variations in Mg content nor appreciable amounts of other elements were observed.

Calcite is sensitive to radiation damage during HRTEM investigations, and so rapid operation was required. To minimize the damage, it was useful to prepare calcite sections having the desired [100] and [001] orientations for imaging. We used θ scans to find these orientations.

SAED patterns of certain regions reveal weak c-type extra reflections (Reeder and Wenk, 1979) halfway between the fundamental calcite reflections (Fig. 5a). We found that the intensities of the c reflections vary considerably from place to place. Images obtained from areas in which the c reflections are most pronounced contain round domains exhibiting a set of parallel, widely spaced fringes that suggest a superstructure. These domains are <10 nm in diameter (Fig. 6). The orientations of the superstructure fringes in different domains appear to be rotated by 120° to one another, as would be expected if their orientations were controlled by the host carbonate. An SAED pattern and image of diagenetic magnesian calcite from a Jurassic ammonite, similar to Figures 5a and 6, are shown by Wenk et al. (1991).

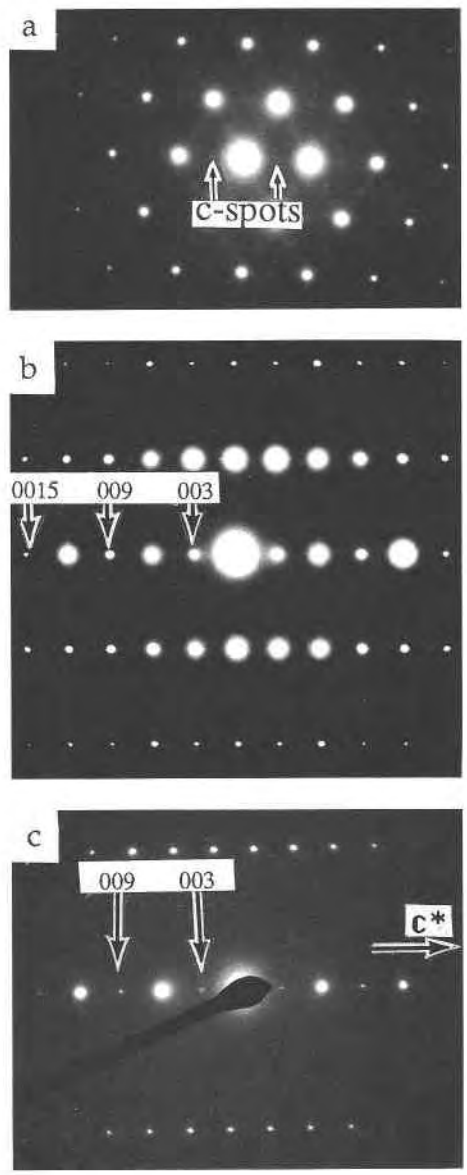

Fig. 5. SAED patterns of the same *Str. fr.* spine as is illustrated in Fig. 3. The projections are along (**a**) [001], (**b**) [100], and (**c**) [120]. The arrows show the positions of superstructure spots.

In contrast to SAED patterns of magnesian calcite from sediments (Wenk et al., 1991), some of our [100] and [120] SAED patterns contain dolomite-like 00*l* reflections, such as 003, 009, and 0,0,15 (Fig. 5b, 5c). Tilting experiments were performed to determine whether they might arise from dynamical effects. Although they became weaker and so may have some dynamical contribution, these reflections were not eliminated by tilting, and therefore they are at least permissive of $R\bar{3}$ or lower symmetry. Moreover, since these same reflections were

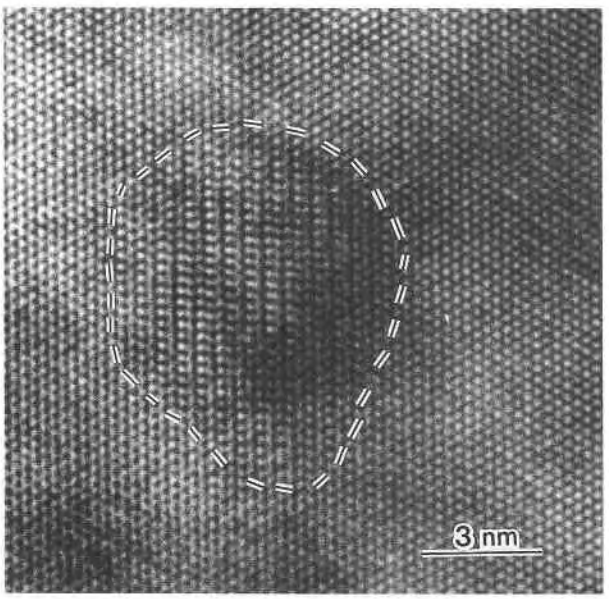

Fig. 6. A [00*l*] image of the *Str. fr.* spine. The outlined region shows one of the domains that displays an ordered superstructure.

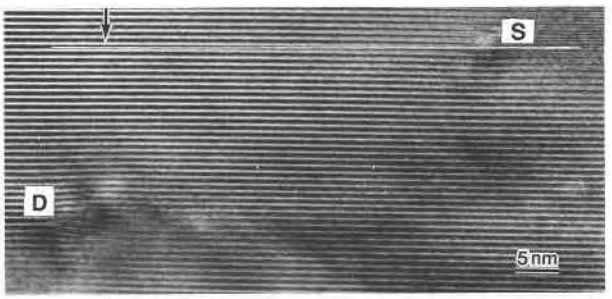

Fig. 7. A [100] image of a slightly bent crystal of the *Str. fr.* spine. Reference to the white line (arrowed) shows the misalignment. A region of strain (S) and a dislocation (D) are indicated.

observed in the X-ray patterns, we believe that they are real and thereby indicate the presence of dolomite-like structure, rather than simply being the result of multiple diffraction.

We found numerous instances of crystal misorientations within the urchin calcite similar to those observed by Blake et al. (1984), who described a coherent boundary between two slightly misoriented blocks in magnesian calcite. Local areas of strain and dislocations are associated with such misorientation, as seen in [100] projection (Fig. 7).

Our samples also contain crystallographic defects that produce incoherent domains. These defects include stacking faults (Fig. 8a), dislocations, and complicated planar defects of composite character that seem to be typical of the urchin calcite. Figure 8b shows examples of elongate, slightly winding defects that cut across regions of well-formed calcite from *Str. fr.* Calcite from *Str. pr.* also displays such long (>130 nm) subgrain boundaries (Fig. 8c).

Discussion

Both the diffraction patterns and HRTEM images of our samples indicate the presence of superstructural domains in regions ~10 nm in diameter. Superstructures have been reported from many diagenetic rhombohedral carbonates (Reeder and Wenk, 1979; Gunderson and Wenk, 1981; Van Tendeloo et al., 1985; Wenk and Zhang, 1985; Frisia Bruni and Wenk, 1985; Miser et al., 1987; Barber and Khan, 1987; Reksten, 1990a, 1990b).

Wenk et al. (1991) proposed several ordering models to explain the superstructures in magnesian calcite. Four of their models result in a doubling of the a_1 and a_2 cell dimensions. Figure 9a and 9b provide perspective views and [001] projections of the ν and γ models that are of special interest for our purposes. It is convenient to discuss them with reference to calcite (α structure) and dolomite (β structure). In dolomite the Ca and Mg cations lie in layers that alternate along **c**. Each cation layer in the ν structure has a composition with the dolomite ratio of Ca:Mg = 1:1 and contains rows of Ca and rows of Mg alternating along one of the hexagonal **a** axes. Thus, all layers in the ν structure are compositionally identical, whereas those of dolomite are compositionally distinct. The γ structure can then be described as a composite of the calcite and ν structures, with a regular alternation of Ca layers and Ca and Mg layers along [001], resulting in Ca:Mg = 3:1. The γ structure can also be considered as a composite of the dolomite and ν structures, with all Mg layers of dolomite replaced by ν-type layers. As in dolomite, adjacent layers have different compositions.

Figure 9c shows simulated [001] images. For this orientation, the several models yield distinct ordering patterns and diffraction patterns. In distinction to the identical cation site occupations and hexagonal organization of the cations in calcite and dolomite, the ν and γ models show doubled spacings along one of the **a** axes and nonhexagonal ordering. Such doubling and ordering are compatible with the domains in Figure 6 and presumably give rise to the c reflections in Figure 5a. They occur in three directions as a result of the several orientations of the domains within the host calcite (Reeder, 1992).

The simulated [001] images of the γ and ν models appear similar (Fig. 9c), as do their [001] diffraction patterns. However, for orthogonal orientations, their diffraction features differ. Specifically, the γ structure yields odd 00*l* (003, 009, . . .) reflections (as does dolomite), whereas the ν structure does not. The X-ray data suggest two distinct *c* parameters, 1.696 and 1.662 nm, corresponding to calcite containing minor Mg and to carbonate containing an increased amount of Mg, respectively. The odd 00*l* reflections seen in X-ray and SAED patterns, taken together with the experimental and simulated HRTEM images, suggest that the domains in our material have the γ structure. However, we cannot exclude the possibility that regions having the ν structure could also exist, given that

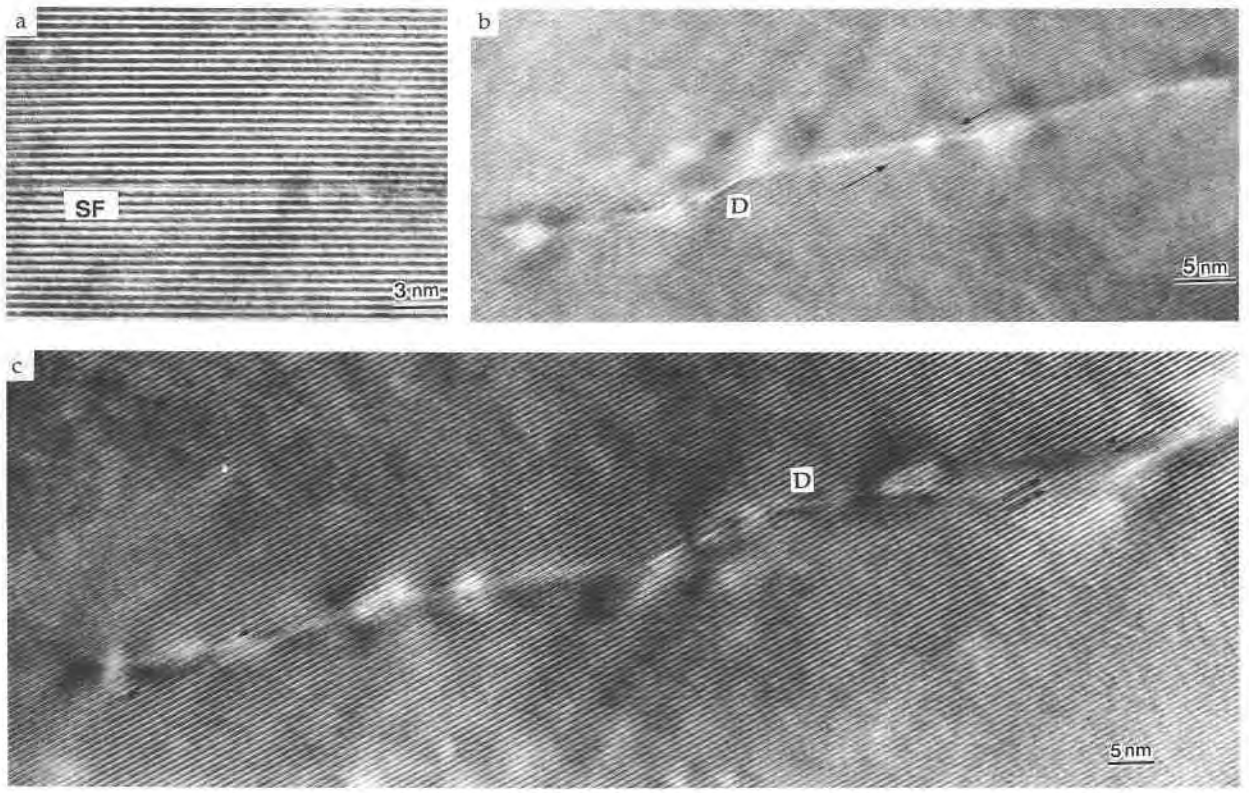

Fig. 8. Three [100] images of subgrain boundaries. (**a**) A stacking fault (SF) and (**b**) misaligned blocks characterized by offset fringes on opposite sides of the subgrain boundary of a *Str. fr.* spine, (**c**) a long (>130 nm) defect zone separating two mosaic blocks in a *Str. pr.* spine. The arrows show shifts in the fringe contrast. A dislocation (D) is indicated.

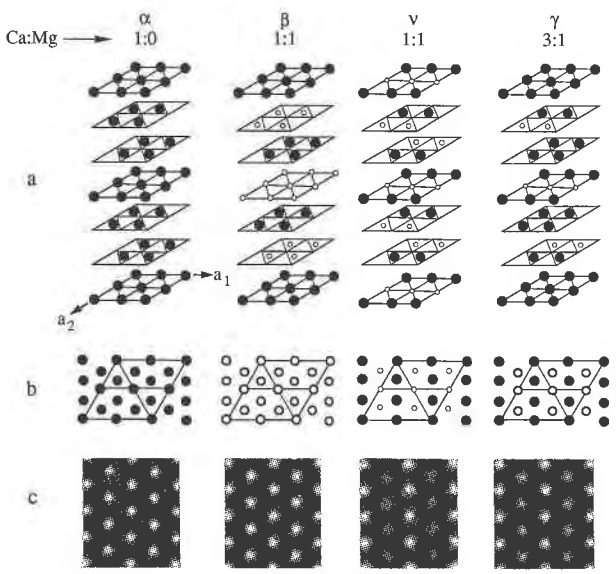

Fig. 9. The effects of different Ca and Mg ratios on the carbonate structure. (**a**) Models showing different ordering schemes and the corresponding (**b**) [001] projections, and (**c**) computer simulated images (Scherzer focus). The scale of **c** is 1.33 times that of **b**. The large solid circles represent Ca, the small open circles indicate Mg, and the large open circles indicate columns containing both Ca and Mg; CO_3 is not shown.

their diagnostic features are not unique where ν occurs together with γ.

Our conclusion contrasts with the analysis of Wenk et al. (1991), who indicated the ν structure is plausible and the γ structure is prohibited as domains within calcite. They point out that γ can occur within dolomite and can also occur as a secondary ordering product of ν, although they indicate that origin is unlikely. Wenk et al. (1991) studied material that had been diagenetically processed and found the γ structure as domains only within dolomite and the ν structure within magnesian calcite. On the other hand, we investigated biogenic calcite that had not experienced any geological processing and observed the γ structure as domains within calcite. Our results, although complementary to theirs, differ and are incompatible with their theoretical analysis of possible transformations of the structure models. The difference in origin of the two sets of samples may contain the answer to this apparent discrepancy, but a resolution remains in the future.

Our X-ray and HRTEM studies show that a pronounced mosaicism is characteristic of urchin carbonates. Blake et al. (1984) speculated that the "mosaic structure [of biogenic calcite] is a result of small changes in the orientation of submicrometer-sized crystallites, which despite their differences in orientation, are largely coher-

ent." Finding an absence of dislocations, these authors concluded that "the structure is in a state of stress." Our investigations of the imperfections in biogenic calcites show numerous coherent and complex incoherent boundaries between slightly misoriented mosaic blocks (Figs. 7, 8, and 9). Most of these defect zones contain dislocations that relieve stresses in the structure.

There are several possible explanations for the development of mosaicism during crystal growth. Davies et al. (1972) showed that multiple long, thin spines develop in parallel packets and are subsequently connected by narrow bridges of calcite. He concluded that growth is not synchronous across the crystals. Moreover, localized environmental conditions have a profound influence on the perfection of the skeletal hard parts of sea urchins. Their growth rate and Mg content depend on the temperature of the sea water and the food supply (Weber, 1969; Davies et al. 1972; Pearse and Pearse, 1975). Deviations in these conditions are reflected in the internal structure of the hard parts and may result in uneven crystal growth and mosaic structures with intermediate defective zones, in spite of strong organismal control. Contrary to the results of Berman et al. (1990), we found no evidence of organic matrix either along the subgrain boundaries or within the calcite structure.

It is apparent that our biogenic calcite, which has not been processed geologically, and material that has undergone diagenesis (Wenk et al., 1991) show different features. It remains for a future study to determine how general these differences are and whether they arise from aging or from other processes.

Acknowledgments

Samples of *Str. fr.* were kindly provided by D. Chandler of Arizona State University (ASU) and those of *Str. pr.* from Marinus, Inc. (Long Beach, California). We thank A. Berman and K. Towe for reprints as well as samples and R. Reeder, K. Towe, and R. Angel for helpful reviews. This study was supported by NSF grant EAR-87-0529. The X-ray and electron microprobe investigation was performed in the Department of Chemistry, and electron microscopy was done at the ASU Facility for HREM, which is supported by NSF and ASU. The electron microprobe was purchased with the aid of NSF grant EAR-84-08163. We are especially grateful to those families who provided private donations to help support the research of S.J.T. at ASU.

References cited

Azároff, L.V., Kaplow, R., Kato, N., Weiss, R.J., and Young, R.A. (1974) X-ray diffraction. In International Series in Pure and Applied Physics, 664 p. McGraw-Hill, New York.

Barber, D.J., and Khan, M.R. (1987) Composition-induced microstructures in rhombohedral carbonates. Mineralogical Magazine, 51, 71–78.

Berman, A., Addadi, L., Kvik, A., Leiserowitz, L., Nelson, M., and Weiner, S. (1990) Intercalation of sea urchin proteins in calcite: Study of a crystalline composite material. Science, 250, 664–667.

Blake, D.F., Peacor, D.R., and Allard, L.F. (1984) Ultrastructural and microanalytical results from echinoderm calcite: Implications for biomineralization and diagenesis of skeletal material. Micron and Microscopica Acta, 15, 85–90.

Burkhardt, A., and Märker, K. (1979) Statics of the primary spines of Diadematidae. Proceedings of the European Colloquium on Echinoderms, Brussels, 1979, 85–87.

Currey, J.D. (1975) A comparison of the strength of echinoderm spines and mollusc shells. Journal of Marine Biology Association, 55, 419–424.

Currey, J.D., and Nichols, D. (1967) Absence of organic phase in echinoderm calcite. Nature, 214, 81–83.

Davies, T.T., Crenshaw, M.A., and Heatfield, B.M. (1972) The effect of temperature on the chemistry and structure of echinoid spine regeneration. Journal of Paleontology, 46, 874–883.

Donnay, G., and Pawson, D.W. (1969) X-ray diffraction studies of echinoderm plates. Science, 166, 1147–1150.

Emlet, R.B. (1982) Echinoderm calcite: Mechanical analysis from larval spines. Biological Bulletin, 163, 264–275.

Frisia Bruni, S., and Wenk, H.R. (1985) Replacement of aragonite by calcite in sediments from the San Cassiano formation (Italy). Journal of Sedimentary Petrology, 55, 159–170.

Gunderson, S.H., and Wenk, H.R. (1981) Heterogenous microstructures in oolitic carbonates. American Mineralogist, 66, 789–800.

Kleyn, L., and Currey, J.D. (1970) Echinoid skeleton: Absence of collagenous matrix. Science, 169, 1209–1210.

Lowenstam, H.A., and Weiner, S. (1989) On biomineralization, 324 p. Oxford University Press, New York.

Miser, D.E., Swinnea, J.S., and Steinfink, H. (1987) TEM observations and X-ray crystal structure refinement of a twinned dolomite with a modulated microstructure. American Mineralogist, 72, 188–193.

Nissen, H.V. (1969) Crystal orientation and plate structure in echinoid skeletal units. Science, 166, 1150–1152.

O'Neil, P.L. (1981) Polycrystalline echinoderm calcite and its fracture mechanics. Science, 213, 646–648.

Paquette, J., and Reeder, R.J. (1990) Single-crystal X-ray structure refinements of two biogenic magnesian calcite crystals. American Mineralogist, 75, 1151–1158.

Pearse, J.S., and Pearse, V.B. (1975) Growth zones in the echinoid skeleton. American Zoology, 18, 731–753.

Raup, D.M. (1966) The endoskeleton. In R.A. Boolootian, ed., Physiology of echinodermata, p. 379–395. Interscience, New York.

Reeder, R.J. (1992) Carbonates: Growth and alteration microstructures. In Mineralogical Society of America Reviews in Mineralogy, 27, 381–424.

Reeder, R.J., and Wenk, H.R. (1979) Microstructures in low temperature dolomites. Geophysical Research Letter, 6, 77–80.

Reksten, K. (1990a) Superstructures in calcian ankerites. Physics and Chemistry of Minerals, 17, 266–270.

——— (1990b) Superstructures in calcite. American Mineralogist, 75, 807–812.

Towe, K.M. (1967) Echinoderm calcite: Single crystal or polycrystalline aggregate. Science, 157, 1048–1050.

Van Tendeloo, G., Wenk, H.R., and Gronsky, R. (1985) Modulated structures in calcian dolomite: A study by electron microscopy. Physics and Chemistry of Minerals, 12, 333–341.

Weber, J.N. (1969) The incorporation of magnesium into the skeletal calcites of echinoderms. American Journal of Science, 267, 537–557.

Wenk, H.R., and Zhang, F. (1985) Coherent transformation in calcian dolomites. Geology, 13, 457–460.

Wenk, H.R., Meisheng, H., Lindsey, T., and Morris, J.W., Jr. (1991) Superstructures in ankerite and calcite. Physics and Chemistry of Minerals, 17, 527–539.

Yukino, K., and Uno, R. (1986) "ϵ-scanning": A method of evaluating the dimensional and orientational distribution of crystallites by X-ray powder diffractometer. Japanese Journal of Applied Physics, 25, 661–666.

Manuscript received September 25, 1992
Manuscript accepted April 4, 1993